Supermode noise suppression of the harmonically mode-locked fiber laser through continuous wave injection. Experiment and numerical simulations

D.A. Korobko[a], V.A. Ribenek[a], P.A. Itrin[a], I.S. Panyaev[a], P.P. Mironov[a] and A.A. Fotiadi[a, b]
[a]Ulyanovsk State University, 42 Leo Tolstoy Street, Ulyanovsk, 432970, Russian Federation
[b]Electromagnetism and Telecommunication Department, University of Mons, Mons, B-7000, Belgium

ABSTRACT

We report on the results of experimental and numerical studies enabling deep insight into the physical mechanisms underlying the supermode noise suppression in harmonically mode-locked (HML) fiber laser using the resonant continuous wave (CW) injection. In particular, we have proved experimentally that the supermode noise suppression effect is available only with the CW injected to the long-wavelength side of laser spectrum. Injection to the opposite side destroys the HML operation regime and leads to the formation of tight soliton bunch. Our numerical simulations confirm these specific features. To get the result, we have simulated phase-locking between the CW and a single soliton. Then, the developed model has been applied to the laser cavity operating multiple pulses in the presence of the gain depletion and recovery mechanism responsible for harmonic pulse arrangement. We clearly demonstrate how the CW injection accelerates or destroys the HML process enabling the generation of additional inter-pulse forces.

1. INTRODUCTION

Ultra-fast laser sources delivering pulses with the pulse repetition rate (PRR) in sub-GHz and GHz range are of great interest for many applications in spectroscopy, microwave photonics, ranging sensing, telecommunications, etc. [1-6]. Mode-locked fiber lasers have become a valuable alternative to semiconductor and solid-state lasers ensuring high beam quality, simplicity in adjustment, reliability, user-friendly light output, all inherent to the laser configurations spliced in all-fiber format. Since the fundamental PRR of the mode-locked lasers is determined by the cavity length, it is limited by hundreds of MHz for the fiber lasers of standard cavity length. In the harmonic mode-locking (HML) regime the multiple pulses are evenly spaced inside the cavity and the laser emits regular pulses with much higher PRR equal to an integer multiple of the fundamental PRR [6-10]. The HML could be implemented in the fiber laser cavity using a special intra-cavity periodic filter [8, 11-13] or through active mode-locking procedure [14, 15]. However, the most attractive way is the use of the passive harmonic mode-locking mechanism exploiting the pulse repulsion in the ring laser cavity [6-8, 12-18]. A wide range of passive HML laser configurations employing either real (SESAM, carbon nanotubes, etc.) or artificial (nonlinear polarization rotation, Kerr lens, etc.) saturable absorbers have been employed with the HML fiber lasers providing PRR up to tens of GHz [19-22]. The main drawback of the HML laser technology is the noise-induced irregularities of the time interval between the delivered pulses known as the HML timing jitter. Generally, its value is much higher than that of the lasers operating fundamental mode-locking [23, 24]. Therefore, physical mechanisms enabling jitter reduction in HML fiber lasers are of great practical importance [24-30]. The role of continuous wave (CW) injection as a mediator providing the equalizing interaction between pulses has been intensively discussed in this context [24, 25, 28-31].

Recently, we have demonstrated a new technique enabling the mitigation of the supermode noise (and timing jitter) in a soliton HML fiber laser built on the nonlinear polarization evolution (NPE) [24]. In that experiment, an optical injection of an external CW component into the laser cavity causes a suppression of HML laser supermode noise (evaluated through the supermode suppression level (SSL)) by two-three orders of magnitude. In contrast to other earlier studies, the CW injection into the HML lasers, the reported effect exhibits a strong resonant dependence on the CW wavelength and makes no further impact on other laser performance characteristics. Specifically, this effect has been observed at rather exotic experimental conditions determining positions of the injected narrowband CW component and a soliton Kelly sideband within the transmission bands of the ring cavity. To get the effect the laser should be adjusted to put one of the Kelly sidebands near the transparency peak of the birefringent fiber filter formed in the laser ring cavity. Besides the proper laser adjustment, the CW wavelength should be taken within the selected transparency peak. When the CW is injected, the

Nonlinear Optics and its Applications 2024, edited by John M. Dudley, Anna C. Peacock, Birgit Stiller, Giovanna Tissoni, Proc. of SPIE Vol. 13004, 1300410
 · 0277-786X · doi: 10.1117/12.3022122

soliton spectrum as a whole shifts in such a way that the Kelly sideband moves towards the CW component and merges with it. The super-mode noise level drops down immediately after. Thus, the effect is always accompanied by the shift of soliton spectrum. Basing on this observation the following simplified view on the super-mode noise mitigation effect has been suggested. A shift of the soliton carrier frequency occurs due to phase-locking between the soliton and the CW component that in some sense works as the dispersive wave generated by the soliton. It is known that the soliton spectrum frequency shift provokes an accelerated evolution of the perturbed HML system to an equilibrium state improving the regularity of pulse arrangement in the cavity [6, 11, 18]. Although this understanding has no contradiction with the reported experimental observations, neither theory nor numerical simulations have been presented until now to prove or disprove the hypothesis and model the underlying mechanisms. Besides, one can note some intrigue kept in the reported experimental results [24]: the shift of the soliton spectrum has been reported with any selected Kelly sideband, whereas the noise mitigation effect seems to be observable with long-wavelength Kelly sidebands only.

First series of simulations is performed to describe a single soliton propagating in the laser cavity. We consider the dynamics of the soliton and CW interaction exploring a change of the Kelly sideband position towards the injected CW frequency resulting in solid phase-locking between them with formation of the coupled CW + soliton light structure. Second series of simulations is applied to describe the laser configuration operating multiple pulses. In particular, we consider the laser operation in the presence of the gain depletion and recovery mechanism [17] responsible for the equalization of the pulse distribution along the cavity. Then we demonstrate clearly how the CW injection could accelerate or slow down the pulse equalization process by means of generation of additional inter-pulse forces. The results of the numerical simulations are in good agreement with the experimental results. In general, the proposed approach gives a clear insight into the origin of the super-mode noise mitigation caused by the CW injection.

2. EXPERIMENT

The noise mitigation effect in HML laser has not been demonstrated with the CW injected into a short-wavelength side of the laser spectrum. Indeed, such CW injection gives an effect very different from the expected one. In this section, we present new experimental studies highlighting these properties. The experimental configuration of an Er-doped soliton NPE mode-locked fiber ring laser is shown in Fig. 1 and it is not so different from the previous laser setup [24]. The laser cavity consists of two types of fiber: 0.8 m length of heavily erbium-doped fiber (EDF) with normal dispersion (-48 ps/nm/km) and standard single mode

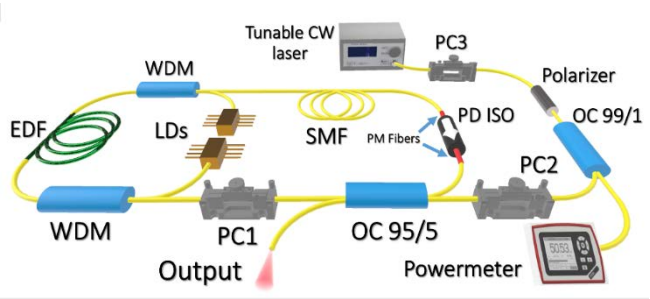

Fig. 1. Experimental HML laser setup.

fiber (SMF-28) with anomalous dispersion (17 ps/nm/km). The total length of the laser cavity of 15.5 m corresponds to the fundamental PRR $f_0 = 14.1 MHz$. Polarization-dependent fiber isolator (PD ISO), two 980/1550 WDM couplers, in-line polarization controller (PC1), and 5% output coupler (OC) are incorporated into the cavity. The laser is pumped at 980 nm from two laser diodes specified for the maximum power of 550mW.

The central wavelength of the soliton laser operation can be selected by a rough PC1 adjustment from a few spectral bands between 1550 and 1590 nm specific for the built fiber configuration. The light from the external tunable PM laser source "Yenista T100" is used for injection into the laser cavity. The CW laser is tunable in the range of 1550-1590 nm and set to operate with the linewidth of ~ 100 kHz and output power of ~ 3.5 mW. The polarization controllers PC2 and PC3 are used for independent control of the injected CW polarization state and power, respectively. With the built laser configuration, PC2 is adjusted once for maximal transparency of the fiber cavity to the injected light and then kept fixed. The injected CW power is smoothly controlled by PC3 and monitored by the photodiode (Fig.1). The laser operation is

monitored by an optical spectrum analyzer (Yokogawa 6370D) with resolution of 0.02 nm and RF spectrum analyzer (R&S FSP40) coupled with a 30 GHz photodetector.

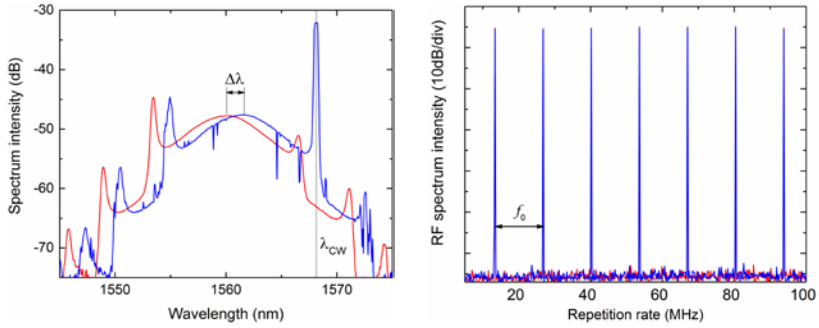

Fig. 2. Optical (a) and RF (b) spectra recorded with the FML fiber laser before (red curve) and after (blue curve) the CW injection at PRR=f_0 ~14.1 MHz. One of the FTM bands is close to the long wavelength Kelly sideband. The gray line shows the CW spectral position within the FTM band. The optical spectrum shift is depicted. RF spectra have been recorded in a 100 MHz span with a 200 kHz resolution. It does not change with the CW injection.

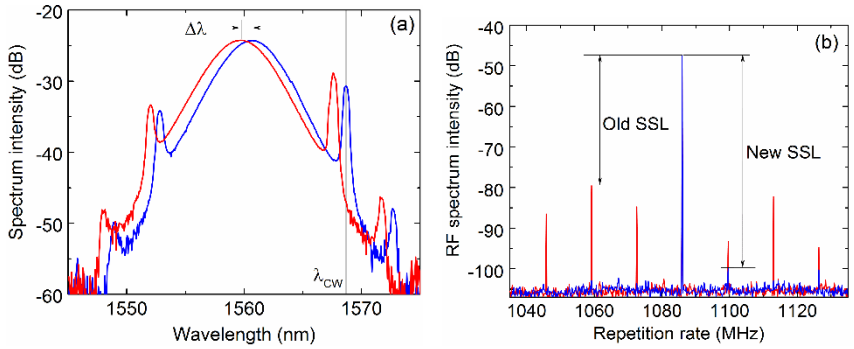

Fig. 3. Optical (a) and RF (b) spectra recorded with the HML fiber laser before (red curve) and after (blue curve) the CW injection at PRR ~1.084 GHz. The CW component is close to the long wavelength Kelly sideband. The optical spectrum shift and the SSLs before and after the CW injection are also depicted. RF spectra have been recorded in a 100 MHz span with a 200 kHz resolution. The gray line shows the CW spectral position within one of the FTM bands.

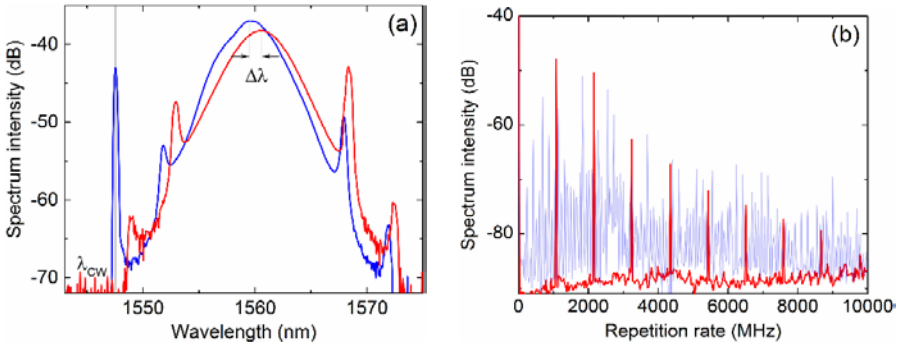

Fig. 4. Optical (a) and RF (b) spectra recorded with the HML fiber laser before (red curve) and after (blue curve) the CW injection at initial PRR 1.084 GHz. The CW is close to the short wavelength Kelly sideband. The optical spectrum shift is also depicted. RF spectra have been obtained in a 10 GHz span with a 30 MHz resolution. The gray line shows the CW spectral position within one of the FTM bands.

Without optical injection, the laser operation is typical for HML lasers based on the NPE mechanism. In our experiment, the laser operating wavelength is set to λ ~ 1559 nm. Once the lasing threshold (30 mW) is achieved the fundamental mode-locking (FML) regime is established. At a low pump power level (~80 mW) the laser still operates in FML regime

generating regular pulses with the fundamental PRR f_0. In this regime, only a single soliton pulse circulates inside the laser cavity. With an increase of the pump power the laser switches to multi-pulse operation. A delicate adjustment of PC1 at this stage equalizes distribution of the generated pulses inside the cavity thus enabling the HML operation regime. In the HML regime, the laser emits regular pulses with the PRR equal to N pulses per cavity round trip, $f_{rep} = Nf_0$. The PRR could be increased by an increase of pump power. Besides, at each pump power level the PRR could be also tuned by fine adjustment of PC1.

The fiber birefringence (Lyot) filter formed by PC1, SMF-28 and PD ISO inside the ring cavity plays a crucial role in our observations. The spectral transmittance peaks of the filter are spaced periodically and for the reported laser implementation are centered around the wavelengths λ ~ 1547 nm, 1557.5 nm, 1568 nm, 1579.5 nm. Narrow (< 1 nm) bands centered at these wavelengths are referred hereafter to as the filter transmittance maximum (FTM) bands. The effect of the CW injection on the laser behavior does depend on the position of the FTM bands in respect to the laser optical spectrum [24]. Figures 1-3, a show examples of the laser optical spectrum measured in different laser operation regimes. Specifically, all spectra are featured by pronounced Kelly sidebands generated at both spectrum wings. With a properly adjusted laser one of the Kelly sidebands should be arranged close to an FTM band. To get the effect than, the CW light should be injected to the selected FTM band. The details on laser adjustment procedure are given in [24] (supplementary materials).

The effects of the CW light injection on the laser behavior have been evaluated through the monitoring of the laser optical and RF spectra. The spectra presented in Figs. 1 - 3 are obtained with the properly adjusted laser. Figures 2 shows the spectra recorded with the laser operating fundamental mode-locking (FML), i.e. with the PRR equal to f_0. The total pump power is ~500 mW. One can see that the optical spectrum shown in Figs. 2(a, red curve) has one long-wavelength Kelly sideband located near an FTM band. The effect is highlighted by direct comparison of the spectra obtained before (red curves) and after (blue curves) the optical injection. When CW is injected to this FTM band, the soliton spectrum shifts as a whole by $\Delta\lambda \approx 1.3\,nm$ and the Kelly sideband moves towards the CW line and merges with it. The corresponding RF spectra shown in Figs.2(b) constitutes the peaks of equal amplitudes that are equally spaced with a step equal to the PRR. The peak/background contrast exceeds ~100 dB thus manifesting a low timing jitter that is typical for the FML lasers. (A similar effect can be observed with the CW injection into the short-wavelength Kelly sideband as its coincidence with one of the FTM band is provided by laser adjustment). Importantly, no modification of the RF spectra is observed with the CW light injection into the laser cavity operating with the fundamental PRR.

Figures 3, 4 demonstrate the result of CW light injection into the laser operating in HML regime. The optical spectrum shown in Figs. 2(a, red curve) has one long-wavelength Kelly sideband located near an FTM band. The CW is injected to this FTM band. Similar to Fig.1, when the CW is injected, the soliton spectrum shifts as a whole by $\Delta\lambda \approx 1.3\,nm$ and the Kelly sideband moves towards the CW line and merges with it. Importantly, in the case of HML laser operation, the CW injection affects the RF laser spectrum as well. One can see that the super-mode noise level drops down by 25 dB (from -30dB down to -55 dB) immediately after the injection highlighting the noise mitigation effect. It worth noting that the effects depend on the injected CW power. A gradual decrease of the injected power down to ~ 0.3 mW reduces the SSL and frequency shift simultaneously. At ~ 0.3 mW and lower, the SSL gets its original value of 30 dB and no frequency shift occurs.

The optical spectrum shown in Figs. 3(a, red curve) has one short-wavelength Kelly sideband located near an FTM band. When the CW is injected into this FTM band, the soliton spectrum shifts by $\Delta\lambda \approx 1.3\,nm$ similar to that shown in Fig.2 and the Kelly sideband merges with the CW line. However, the changes of the RF spectrum shown in Fig.3(b) drastically differ from that expected with the noise mitigation effect. One can see that in this case the CW injection completely destroys periodicity of the RF spectrum, producing a lot of extra spikes and noisy fluctuations instead. Such RF spectrum highlights a stop of HML laser operation and transition to another operation mode.

In conclusion to this section, we have proved experimentally that the side of the laser spectrum where the Kelly sideband is taken for the resonant CW injection is crucial for implementing the noise mitigation effect. We have shown that improvement of the laser performance characteristics (the supermode noise level, timing jitter) occurs with long-wavelength Kelly sidebands only. On the contrary, the use of short-wavelength Kelly sideband deteriorates the laser performance destroying the HML operation regime. It is worth noting that this drastic difference in the laser evolution does not affect the frequency shift that always accompanies both effects independently of the side the CW is injected. Besides, a similar frequency shift effect is observed with the laser operating in FML regime.

In the next sections, we present the mathematical model and results of numerical simulations providing a solid explanation of the observed features.

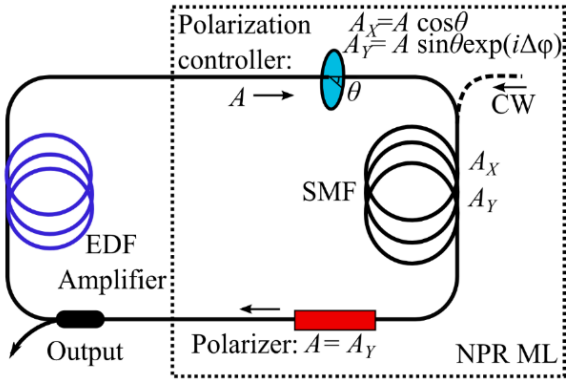

Fig.5. The scheme of laser setup used in simulations. The dotted line defines the block responsible for the laser mode–locking.

3. NUMERICAL SIMULATION LASER MODEL

The configuration of fiber ring laser used for numerical analysis is depicted schematically in Fig. 5. It comprises a gain fiber (or EDF amplifier), a polarization controller (PC), a piece of passive single-mode fiber (SMF), a polarizer, and an output coupler. We assume that the light propagating in the gain fiber is linearly polarized, whereas the light propagating in SMF could possess an elliptical polarization. For this reason, a negligibly low fiber birefringence is assigned to the passive fiber and the polarizer is used for modelling the polarization-dependent optical isolator shown in Fig.1. A number of the cavity characteristics such as dispersion, nonlinearity and fiber gain factor are defined by their net cavity values and considered to be uniformly distributed over corresponding fiber segments.

The light propagation through the laser cavity is described by the nonlinear Schrodinger (NLS) type equations. An evolution of the optical field amplitude in the gain fiber is governed by the generalized NLS equation:

$$\frac{\partial A}{\partial z} - i\frac{\beta_{2g}}{2}\frac{\partial^2 A}{\partial t^2} - i\gamma_g |A|^2 A = \frac{gA}{2} + \frac{g}{2\Omega_g^2}\frac{\partial^2 A}{\partial t^2}, \qquad (1)$$

where, A is the complex amplitude of the linearly polarized electric field in the gain fiber, z is the coordinate along the fiber, β_{2g} is the group velocity dispersion (GVD), and γ_g is the Kerr nonlinearity of the gain fiber. The gain spectral filtering is centered at λ_0 and employed in parabolic approximation with the FWHM gain line bandwidth Ω_g. The saturated gain factor g is averaged over the simulation window and is expressed as

$$g(z,t) = g(z) = g_0\left(1 + \frac{1}{E_g}\int_0^{\tau_{win}} |A(z,t)|^2\, dt\right)^{-1}, \qquad (2)$$

where g_0 is a small signal gain factor and E_g is the gain saturation energy determined by the pump power, τ_{win} is the width of the simulation window.

The light propagation in the passive single-mode fiber (SMF) is described by the two coupled nonlinear Schrodinger equations:

$$\begin{aligned}
&\frac{\partial A_X}{\partial z} - i\frac{\beta_2}{2}\frac{\partial^2 A_X}{\partial t^2} - i\gamma\left(|A_X|^2 + \frac{2}{3}|A_Y|^2\right)A_X - \frac{i}{3}\gamma A_X^* A_Y^2 = 0,\\
&\frac{\partial A_Y}{\partial z} - i\frac{\beta_2}{2}\frac{\partial^2 A_Y}{\partial t^2} - i\gamma\left(|A_Y|^2 + \frac{2}{3}|A_X|^2\right)A_Y - \frac{i}{3}\gamma A_Y^* A_X^2 = 0,
\end{aligned} \qquad (3)$$

where A_X and A_Y are the field amplitudes of two polarization components. The effects of cross-modulation and four-wave mixing are taken into account by the third and fourth terms in Eq.3. To avoid the effects associated with the fiber

cavity inhomogeneity, the gain fiber and the SMF are assumed to have the same nonlinearity $\gamma_g = \gamma$ and GVD $\beta_{2g} = \beta_2$.

The polarization state of light inside the passive fiber (SMF) is set by the polarization controller (PC) at the fiber input as $A_X = A\cos\theta$, $A_Y = A\sin\theta$, where θ is the angle between the polarization direction of the input light and the fast axis of the SMF, which can be tuned by adjusting the PC. The block combining the PC, SMF and the polarizer operates as a nonlinear "absorber". Its transmission involving NPE is a saturating function of the input signal power $|A|^2$ that at a certain set of parameters ensures the laser mode-locking, providing the generation of an ultrashort pulse [32]. All the linear losses experienced by the signal inside the cavity are taken into account as the local losses in the output coupler described by its power transmission coefficient $\rho^2 : A' = \rho A$.

To study interaction between the solitons propagating in the laser cavity and the injected CW the following expression for the CW light amplitude is used:

$$A_{CW}(t,k) = \sqrt{p_{CW}}\exp\left(i\left(\omega_{CW}t + \beta_2\omega_{CW}^2(l_{SMF}+l_a)(k-1)/2 + \Delta\varphi(k-1)\right)\right), \quad (4)$$

where p_{CW} and ω_{CW} are the power and optical frequency of the CW; l_{SMF} and l_a are the lengths of the SMF and the active fiber, respectively, k is the roundtrip number. The CW component is introduced into the system through the point where the optical field is linearly polarized:

$$A_Y(t,k) = A_Y(t,k-1) + A_{CW}(t,k) \quad (5)$$

To meet the experimental conditions a few limitations are applied to the parameters of Eq.4. The CW light is expected not to generate its own nonlinear effects as its power is too low $p_{CW} \le 0.3$ mW. The CW frequency ω_{CW} is always taken as multiple integers of the frequency grid step Δ_ω . With such restrictions, the injected light defined by Eq.4 is resonant to the ring laser cavity independently of the roundtrip k and used frequency ω_{CW} . Equations (1-5) with the boundary conditions in accordance with Fig. 4 have been numerically simulated employing the split-step Fourier method [33]. The cavity parameters used for calculations are typical for the considered type of the HML laser and listed in Table 1.

Table 1. The system parameters used for calculations

Parameter	Value	Parameter	Value
γ ($W^{-1}m^{-1}$)	0.0033	$\Omega_g/2\pi$ (THz)	7.5
β_2 (ps^2m^{-1})	-0.018	g_0 (m^{-1})	0.2
θ	$(\pi+1)/4$	l_{SMF} (m)	10
$\Delta\varphi$	$\pi/4$	l_a (m)	2.5
ρ	0.95	τ_{win} (ps)	245.76

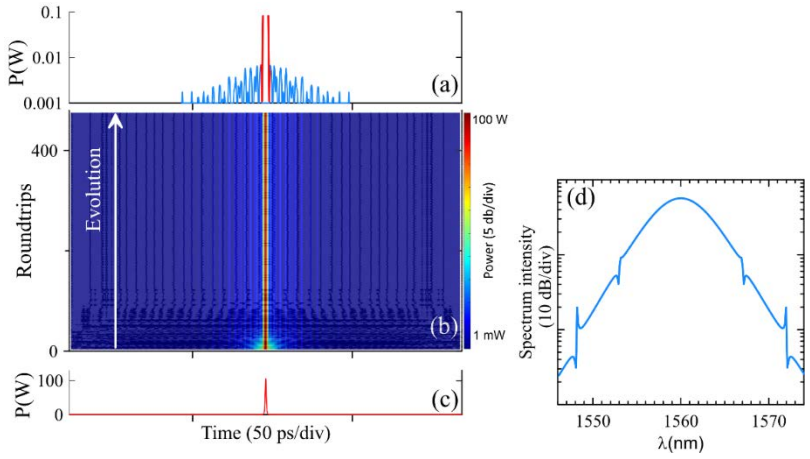

Fig.6. Pulse evolution without CW injection. The saturation energy is $E_g = 20$ pJ. (a) Zoom-in image of the pulse pedestal in a steady-state after 500 roundtrips. (b) Evolution of the pulse and its pedestal. Levels of the constant phase are also shown. (c) Initial conditions shown in a linear scale. (d) Steady-state pulse spectrum.

4. INTERACTION OF A SINGLE SOLITON WITH A NARROW-BAND CW

Without injection of the external CW component, the considered laser model describes dynamics of a soliton fiber laser. With a low-amplitude Gaussian noise used as the initial condition, the laser exhibits self-starting once the parameter E_g exceeds a threshold value ($E_g > 11$ pJ). A single sub-picosecond pulse operation with a typical soliton spectrum is formed inside the cavity after tens of cavity roundtrips.

Fig. 6 demonstrates evolution of the system starting from the instant a single low-power pulse is already generated in the cavity. One can see that the initial pulse position does not change with the roundtrips. It is due to the fact that the fiber dispersion is used in second-order approximation and the results are presented in the co-moving coordinate frame. The laser spectrum is centered at the carrier wavelength $\lambda_0 = 1560\ nm$. The optical spectrum exhibits Kelly sidebands of different orders. They are associated with the dispersive waves generated by the soliton periodically perturbated due to its multiple propagation through the fiber cavity. In the time domain, these dispersive waves are superposed leading to formation of the soliton pedestal highlighted in Fig.6 (a). It is worth noting that the dispersive waves associated with the sidebands of longer wavelengths form the left side of the pedestal, whereas the dispersive waves associated with the sidebands of shorter wavelengths form the right side of the pedestal. In the steady-state the constant phase lines (and the lines of equal intensity) in the pedestal are parallel to the pulse trajectory.

The CW injection may have a pronounced effect on the laser pulse evolution process. When the CW wavelength λ_{CW} is spectrally far from any Kelly sideband, the CW propagation constant β_{CW} greatly differs from the propagation constants of the soliton or a dispersive wave inside the cavity. The simulations show that in this case no significant interaction between the injected CW and soliton laser system occurs. Only small fluctuations of the pulse peak power and rather weak changes of soliton group velocity occur, i.e., the laser system keeps its initial steady-state. When the λ_{CW} approaches a Kelly sideband the fluctuations of the soliton peak power become larger. Closer approaching of the CW component to the Kelly sideband induces a drastic modification of the system evolution. The soliton laser spectrum shifts as a whole in such a way that the Kelly sideband moves towards the CW line and merges with it. This spectrum shift is resulted in the change of the pulse group velocity and in solid phase-locking with formation of the coupled CW + soliton light structure. This process is illustrated in Figs. 7, 8 using $E_g = 20$ pJ and $p_{cw} = 0.2$ mW. One can see how the CW component injected to the right edge of the first order Kelly sideband at $\lambda_{cw} = 1567.79$ nm (Fig. 7 (c)) pushes the Kelly sideband (together with the whole pulse spectrum) to move towards the injected CW frequency. After thousands (N~1500) of cavity roundtrips, the soliton Kelly sideband merges with the injected CW component and the system is transformed into a new steady-state with the soliton spectrum shifted by $\Delta\lambda$ (Fig. 7 (a, b)). Considering the interaction between the CW and the pulse we should conclude that the CW injection near the Kelly sideband creates a local minimum of the interaction potential. The

fall of the pulse to this “potential well” looks like a shift of the Kelly sideband towards the CW frequency followed by their permanent merging.

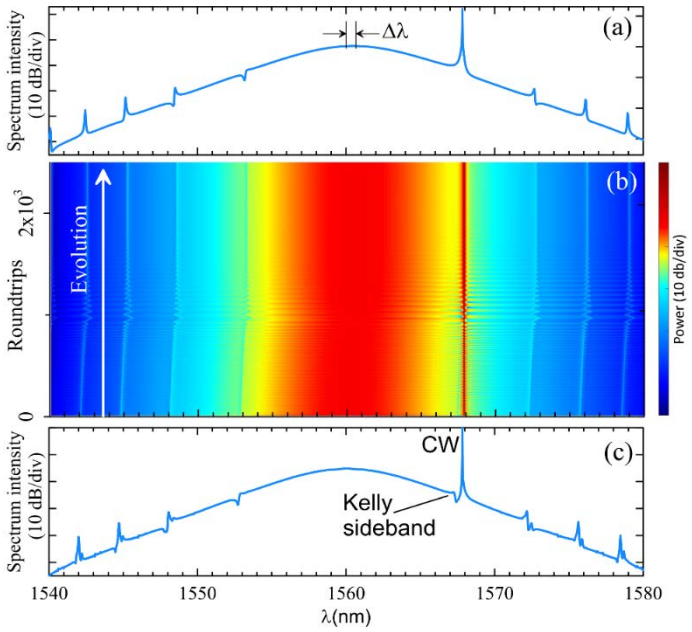

Fig. 7. Evolution of the pulse spectrum with CW injection. The CW wavelength is close to the first-order Kelly sideband. $E_g = 20$ pJ, $p_{cw} = 0.2$ mW, $\lambda_{cw} = 1567.79$ nm (a) The steady-state spectrum of the pulse after 2500 cavity roundtrips. (b) Evolution of pulse spectrum. (c) Initial spectrum of the pulse and injected CW.

Figs. 8 (a-d) show the same evolution of the system presented in the time domain. Initially, the frequencies of the injected CW and dispersive waves are different, so the phase difference between the CW component and dispersive waves varies from a roundtrip to roundtrip (Fig.8(b)). One can see how a low-amplitude background surrounding the soliton pulse fluctuates due to interference of multiple dispersive waves and CW (Fig. 8 (b)). When the CW frequency approaches the Kelly sideband, the interaction between the injected light and soliton increases. One can recognize two kinds of interactions governed by XPM and FWM terms in Eq.3, respectively. For the first N~1500 roundtrips, the XPM term dominates resulting in the amplitude modulation of the soliton pulse shown in Fig. 8 (d). Simultaneously, the FWM gradually redistributes the energy between the soliton cavity modes resulting in a final distribution that does not support anymore the energy transfer from the CW light to the soliton [34]. In other words, the FWM forces the system to get the minimum of the potential energy governing the interaction between the CW and the soliton pulse. At some instant this process is similar to the well-known dissipative FWM effect [14, 35-37]. In the frequency domain, the redistribution of the soliton cavity modes is observed as the shift of the soliton spectrum towards the CW component. In the time domain the frequency shift corresponds to the change of the soliton pulse group velocity. In the used coordinate frame (Fig.8 (b)) it looks like a transformation of the soliton trajectory from a vertical to inclined straight line (please, compare Figs. 6(b) and 8(b)).

However, most importantly, the merge of the Kelly sideband with the CW frequency manifests a strong phase-locking between the injected light and soliton that is pronounced in the time domain [38-40]. One can see, the injected CW occurs to be in anti-phase with the dispersive wave associated with the selected Kelly sideband annihilating it and, on the contrary, the injected CW occurs to be in-phase with the dispersive wave associated with the symmetrical Kelly sideband reinforcing it. In other words, the interacting CW component and soliton are coupled in a single steady-state temporal structure observed in Fig. 8 (a) as an asymmetric pedestal surrounding the soliton pulse. It is worth noting that in the case when the CW approaches the same Kelly peak from the right side, the pulse spectrum shifts to the shorter wavelengths and the pulse trajectory inclines to the right, the steady-state temporal structure, however, remains the same.

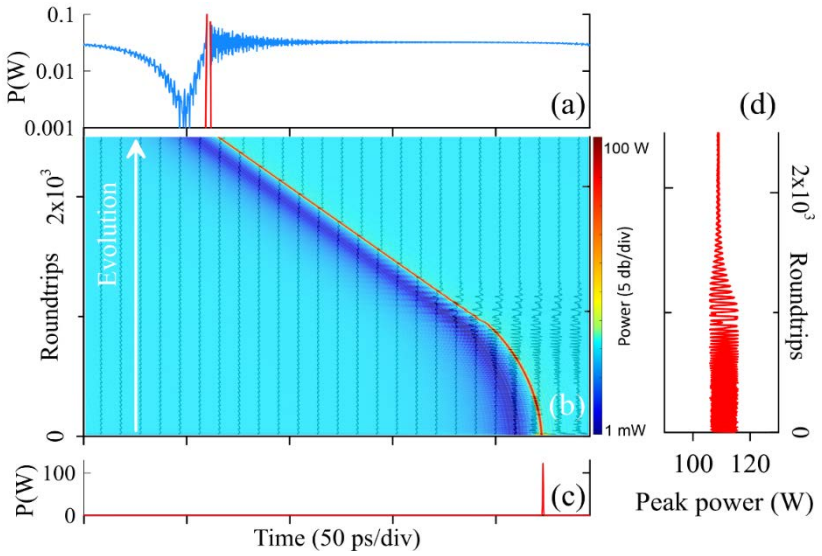

Fig.8. Evolution of the soliton pulse with CW injection. The CW wavelength is close to the first-order Kelly sideband. $E_g = 20$ pJ, $p_{cw} = 0.2$ mW, $\lambda_{cw} = 1567.79$ nm. (a) Zoom-in image of the pulse pedestal in a steady-state after 2500 roundtrips. (b) Evolution of the pulse and its pedestal. Levels of the constant phase are also shown. (c) Initial conditions shown in a linear scale. (d) Variations of the pulse peak power.

To explore the effect of the soliton spectrum frequency shift caused by the CW injection we have performed a series of numerical experiments similar to those shown in Figs. 7-8 but for different values of the gain saturation energy E_g, CW power p_{CW} and wavelength λ_{CW}.

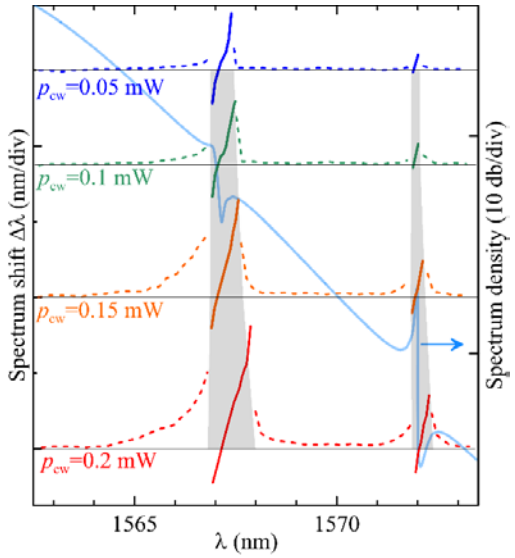

Fig. 9. The pulse spectrum shift as a function of the CW frequency λ_{CW} at different levels of the CW power and $E_g = 20$ pJ. The data corresponding to different p_{cw} are intentionally separated in vertical for better presentation. The horizontal lines for each curve show the zero spectral shift. Within the phase-locking region, the solid lines describe a merge of the Kelly sideband with current CW wavelength. Additionally, phase-locking regions are colored by the gray. Blue line shows the pulse spectrum without shift (at $p_{cw} = 0$).

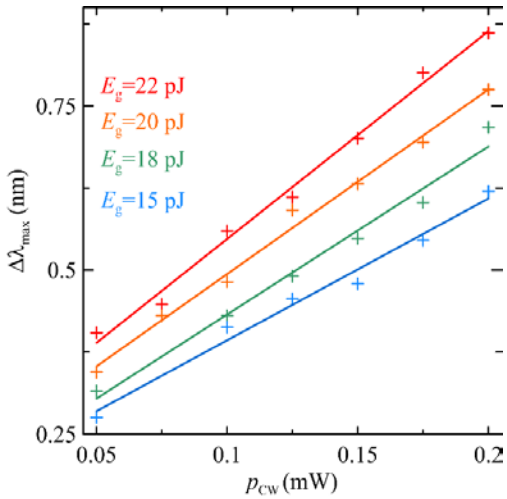

Fig. 10. The maximal shift of the pulse spectrum vs injected CW power p_{cw} for different gain saturation energies E_g (crosses). Solid lines are the approximations of linear dependencies by the method of least squares.

Fig.9 shows the soliton spectrum frequency shift as a function of the selected CW wavelength λ_{CW} obtained at different CW power levels and fixed value of E_g = 20 pJ (i.e., fixed soliton energy). For each set of the parameters, the number of the simulated roundtrips is limited by *N*=5000. One can see that all obtained functions are similar and differ just by maximal and minimal values of the spectral shift that limits the area (colored by gray) where the locking of the Kelly sideband to the CW frequency occurs. We have double checked that in all cases the injection of the CW within these gray areas leads to the soliton spectrum frequency shift followed by phase-locking between the soliton and CW component and formation of the coupled steady-state temporal structure (soliton + CW component). Moreover, when the injected CW catches the Kelly sideband, the soliton spectrum position could be directly.controlled using a slow tuning of the CW frequency within the gray area. It is worth noting that at the given soliton energy, both the width of the phase-locking area and the maximal spectral shift increase almost linearly with the CW power. Besides, the effect is observed with the Kelly sidebands of different orders but the size of phase-locking area decreases with an increase of the sideband order. This feature is explained by much lower amplitudes of the dispersive waves associated with the high-order Kelly sidebands

Fig. 10 shows the maximal soliton spectrum shift (it is equal to the width of phase-locking area (gray) area) as a function of the CW power at different saturation energies E_g (i.e., the soliton energy). One can see the phase-locking area width increases linearly with the power p_{cw} of the injected CW. Besides, the size of the phase-locking area increases with the soliton pulse energy and spectrum width. These facts are in good agreement with our interpretation of the experimental observations suggested earlier [24].

5. MULTI-SOLITON INTERACTION WITH A NARROW-BAND CW

In this section we apply the proposed simulation model to explore the effect of the CW injection on dynamics of several soliton pulses propagating in the ring cavity. Let us first consider the mechanisms underlying the equalization of multi-pulse distribution inside the fiber cavity enabling the HML laser operation. A number of mechanisms responsible for the inter-pulse repulsing inside the cavity have been discussed in this concern [39- 42]. Among them the inter pulse repulsion through gain depletion and recovery (GDR) mechanism are found to dominate in HML laser operating with PRR less than ~20 GHz [2]. To take this mechanism into account a small time-dependent spectrally flat gain described by the standard rate equation has been additionally implemented into the simulation model discussed in the previous sections:

$$\frac{dg_s}{dt} = \frac{g_{0s} - g_s}{\tau_g} - \frac{g_s |A(z,t)|^2}{E_g}, \qquad (6)$$

where g_{0s} is additional small signal gain, E_g is the gain saturation energy and τ_g is the gain relaxation time. The time-dependent gain $g_s(t)$ provides the laser cavity with an additional gain nonuniformity and pushes the pulses to change their mutual position by drifting to the direction of higher gain. The drift velocity of each pulse is proportional to the gain

depletion provided by the pulse. For several identical pulses propagating through the cavity the drift velocity of each individual pulse is determined by the time interval to the preceding pulse in the train. The pulse gets an increase of the drift velocity if this time interval is longer than the averaged one. In this sense, the time-dependent gain induces the inter-pulse repulsion forcing the pulses to rearrange into the regular temporal pattern necessary for the HML laser operation [17]. To simulate the time-dependent gain, the following parameters have been used in Eq. 6: $g_{0s} = 0.0125\,\mathrm{m}^{-1} \ll g_0$ (saturated value of $g_s(t)$ does not exceed 0.2 km^{-1}) and $\tau_g = 7.5$ ns. Although the latter parameter is obviously too small for lasers based on rare earth doped fibers, we use this approach to accelerate simulation demonstrating the effect and having in mind that the condition $\tau_{win} \ll \tau_g$ is still fulfilled. All other system parameters are listed in Table 1.

We have applied our model in combination with the time-dependent gain to simulate the evolution of two pulses in the laser cavity and analyze the effect of the CW injection. Without the time-dependent gain and CW injection both pulses in the cavity experience equal gains and so carry equal energies independently on their mutual position. The injection of CW produces the same effect on both pulses. So, their group velocities change in the same manner and the mutual position of the pulses does not change. When the time-dependent gain is implemented in the laser system, the energy of one pulse becomes dependent on the position of another pulse. They have equal energies only when the pulses are equidistant. If the pulse positions are perturbated, the pulse propagating after longer time interval experiences higher gain getting higher energy. Then, this pulse gets an increase of its group velocity v_{tdg1} that is greater than an increase of the group velocity v_{tdg2} another pulse gets resulting in equalization of the pulse distribution.

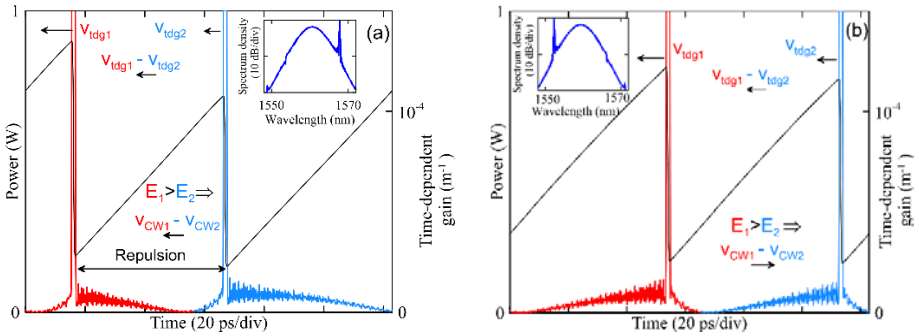

Fig. 11. The interaction of two pulses through the gain depletion and recovery mechanism in the laser cavity with CW injection. The CW frequency is close to the long (a) or short (b) wavelength Kelly sideband. The corresponding laser spectra are in insets.

The injection of CW component into the laser cavity may accelerate or annihilate the pulse equalization process as it is illustrated in Fig. 11. The injection of the CW close to the Kelly sideband induces a frequency shifts to each soliton. However, the soliton possessing higher energy gets higher frequency shift. It is in agreement with the data shown in Fig.10. As a result, the soliton of higher energy acquires higher addition to its group velocity v_{CW1} than v_{CW2} the pulse of lower energy does. The data shown in Fig.11 compare the effect of CW injected close to the first-order Kelly sideband selected from the long-wavelength (a) and short-wavelength (b) sides of the soliton spectrum, all symmetric with the spectrum peak. In the first case, the difference of the group velocities for two pulses acquired due to CW injection has the same sign as the difference of the group velocities provided by the time-dependent gain mechanism. Therefore, two effects support each other and accelerate the equalization of the pulse distribution. In the second case, the group velocity difference is negative and operates against the equalization of the pulse distribution provided by the time-dependent gain mechanism. These results do explain similar effects observed in the experiment.

Finally, we have explored the same equalization process for several soliton pulses propagating in the laser cavity. Fig. 12 compares the system evolution comprising four initially almost equidistant pulses under action of the time-dependent gain alone and in combination with the CW injected close to the long-wavelength first-order Kelly sideband. The use of a short simulation window ($\tau_{win} \approx 246$ ps) equal to the whole cavity length is beneficial for this demonstration. With a short simulation window the inter-pulse distance occurs to be less than in real HML lasers. This fact should be taken into account when interpretating the results. However, it also helps avoid time-consuming calculations. Short inter-pulse distances enhance a noisy interaction between solitons through the dispersive waves they produce. This noisy behavior makes the equalization of the pulse distribution caused by the CW injection even more pronounced. All initial inter-pulse distances

(~60 ps) are close to the perfect HML operation. However, during the evolution the noisy interaction between the pulses tends to impair the quality of HML operation. Figs. 12 (a-c) illustrate how the time-dependent gain operating against the noise managed to keep the pulses equidistantly with an accuracy of ~ 5%. The evolution of inter-pulse distances with time occurs stochastically and sometimes abruptly thus destroying the periodic pulse arrangement. The dynamics of inter-pulse distances well correlate with fluctuations of the pulse amplitudes resulting in a rather high timing jitter (i.e., high supermode noise level). A weak inter-pulse repulsion and randomly varying phase difference between the solitons are commonly considered to be the main reason for the poor HML operation quality.

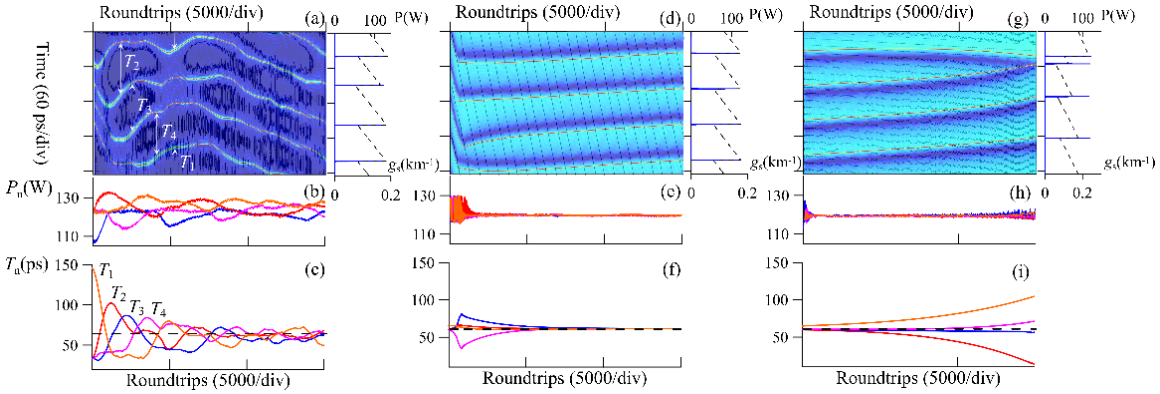

Fig. 12. Comparison of the evolution of four pulses in the system with interpulse repulsion without CW injection (left column - a, b, c) and with CW injection (right column - d, e, f). $E_g = 80\ pJ$, $p_{cw} = 0.2\ mW$, $\lambda_{cw} = 1566.96\ nm$ (a, d) - field evolution into the cavity, the position of the pulses (blue solid lines) and time-dependent gain (dashed lines) after 15,000 cavity roundtrips. The trajectory diagram also shows levels of constant phase. For convenience, the pulse evolution is shown in a moving coordinate frame. (b, e) Changes of the pulse peak powers. (c, f) Changes of the interpulse distances. The dashed line shows the inter-pulse distance corresponding to the HML state.

Figs. 12 (d-f) demonstrate the effect of the CW injection on the first-order long-wavelength Kelly sideband. One can see that the pulse evolution changes drastically. It is due to an increased inter-pulse repulsion inside the cavity provided by the combined action of the CW injection mechanism and the time dependent gain mechanism discussed above. Specifically, the pulse equalization occurs in two steps. In the first step, the CW injection equalization is dominating. The CW injection at one fixed frequency affects each pulse in the train individually introducing a specific carrier frequency shift to each of them. One can see that after phase locking each pulse acquires its own change of the group velocity leading to the equalization of the pulse powers. However, the equalization of the pulse positions is still not achieved. In the second step, all pulses remain phase-locked to a single injected CW component and the time dependent gain mechanism equalizes now the pulse distribution over the cavity resulting in a perfect high-quality HML pulse train generation advancing a low supermode noise level. Completing the picture, the effect of the CW injection on the first-order short-wavelength Kelly sideband is shown in Figs. 12 (g-i). One can see now how the combined action of the CW injection mechanism and the time dependent gain mechanism destroys the HML operation. The first step is similar to the previous case, the dominating CW injection equalizes the pulse powers. However, in the second step, the pulses phase-locked to the injected CW wave suffer from the time dependent gain and recovery mechanism that works against the uniform pulse distribution over the cavity resulting in distortion of the HML pulse train generation. Such simulated HML laser behavior is in good agreement with our experimental observations.

6. CONCLUSION

In conclusion, we have performed experimental and numerical studies providing a clear insight into the physical mechanisms underlying the effect of super-mode noise mitigation in HML fiber laser. A narrow-band CW injected into the laser cavity produces a shift of the soliton spectrum and the super-mode noise level drops down immediately after. In contrast to many rough invasions of the external light to the HML laser, the reported effect makes no impact on the laser performance characteristics. Specifically, the effect exhibits a strong resonant dependence on the CW wavelength and is

observed at very special experimental conditions. New experiments have refined the requirements to the laser adjustment important for the implementation of the supermode noise mitigation effect. It concerns the positions inside the laser spectrum that should be assigned to the injected CW component, a Kelly sideband and the transparency peaks of the birefringent fiber filter. In particular, we have proved experimentally that the side of the laser spectrum from which the Kelly sideband is selected for the resonant CW injection is crucial for the noise mitigation. We have shown that reduction of the supermode noise level occurs with the CW injection close to long-wavelength Kelly sidebands only. On the contrary, the use of opposite Kelly sideband deteriorates the laser performance destroying the HML operation regime. This difference in the laser evolution does not affect the soliton carrier frequency shift that always accompanies both effects independently of the side the CW light is injected.

A standard soliton laser model has been applied to simulate the supermode noise mitigation effect and give explanations to a number of specific features observed in the experiment. First, we have studied the interaction between the CW and a single soliton propagating in the ring cavity. Importantly, we have reproduced in detail the whole soliton laser transition process to the new steady-state. When the CW is injected, the laser soliton spectrum shifts as a whole and the Kelly sideband moves towards the CW light component and merges with it. The carrier frequency shift observed in the spectral domain corresponds to the change of the soliton group velocity in the time domain. We have also established that this merging of the Kelly sideband with the CW light component manifests a strong phase-locking between the injected light and soliton that is very pronounced in the time domain. Then, the developed model has been applied to the laser cavity operating multiple pulses in the presence of the gain depletion and recovery mechanism responsible for periodic pulse arrangement. In particular, we have explained that the supermode noise mitigation effect occurs with the CW injection close to long-wavelength Kelly sidebands accelerating the pulse equalization process by means of generation of additional inter-pulse forces. In contrast, the CW injection to the opposite spectrum side destroys the HML operation regime. The results of the numerical simulations are in good agreement with the experimental results.

We believe that our findings offer important insights into the HML laser dynamics associated with the interaction between the CW and solitons that is crucial for the HML laser design and optimization. The proposed technique can be used to reduce the timing jitter of the HML fiber laser down to the level of lasers operating fundamental mode-locking, thus making the HML lasers promising for an extended range of applications [43-48].

Funding. The work is supported by the Russian Science Foundation (grant # 23-79-30017).

REFERENCES

[1] Diddams S. A., Vahala K., & Udem T., “Optical frequency combs: Coherently uniting the electromagnetic spectrum,” Science 369, 6501 (2020).
[2] Fortier, T. M. and Baumann, E., “20 years of developments in optical frequency comb technology and applications,” Communications Physics 2(1) (2019).
[3] Thurow, B. S., Jiang, N. and Lempert, W. R., “Review of ultra-high repetition rate laser diagnostics for fluid dynamic measurements,” Measurement Science and Technology 24(1), 012002 (2012).
[4] Schliesser, A., Picqué, N., & Hänsch, T. W., “Mid-infrared frequency combs,” Nature photonics, 6(7), 440-449 (2012).
[5] Lesko, D. M., Timmers, H., Xing, S., Kowligy, A., Lind, A. J., & Diddams, S. A., “A six-octave optical frequency comb from a scalable few-cycle erbium fibre laser,” Nature Photonics, 15(4), 281-286 (2021).
[6] Gumenyuk, R. V., Korobko, D. A., & Zolotovskii, I. O., “Stabilization of passive harmonic mode locking in a fiber ring laser,” Optics Letters, 45(1), 184-187 (2020).
[7] Liu, X., & Pang, M. “Revealing the Buildup Dynamics of Harmonic Mode-Locking States in Ultrafast Lasers,” Laser & Photonics Review, 13(9), 1800333 (2019).
[8] Korobko, D.A., Fotiadi, A.A., Zolotovskii, I.O., “Mode-locking evolution in ring fiber lasers with tunable repetition rate,” Optics Express 25(18), 21180-21190 (2017).
[9] Han, Y., Guo, Y., Gao, B., Ma, C., Zhang, R. and Zhang, H., “Generation, optimization, and application of ultrashort femtosecond pulse in mode-locked fiber lasers,” Progress in Quantum Electronics 71, 100264 (2020).
[10] Ribenek, V. A., Korobko, D. A., Fotiadi, A. A., & Taylor, J. R., “Supermode noise mitigation and repetition rate control in a harmonic mode-locked fiber laser implemented through the pulse train interaction with co-lased CW radiation,” Optics letters, 47(19), 5236-5239 (2022).

[11] Rissanen, J., Korobko, D. A., Zolotovsky, I. O., Melkumov, M., Khopin, V. F., & Gumenyuk, R. "Infiltrated bunch of solitons in Bi-doped frequency-shifted feedback fibre laser operated at 1450 nm," Scientific reports, 7(1), 44194 (2017).
[12] Mao, D., Liu, X., Sun, Z., Lü, H., Han, D., Wang, G. and Wang, F., "Flexible high-repetition-rate ultrafast fiber laser," Scientific Reports 3(1) (2013).
[13] Andral, U., Buguet, J., Fodil, R. S., Amrani, F., Billard, F., Hertz, E. and Grelu, P., "Toward an autosetting mode-locked fiber laser cavity," Journal of the Optical Society of America B-optical Physics 33(5), 825 (2016).
[14] Abramov, A., Korobko, D., & Zolotovskii, I., "Frequency Comb Fiber Generator Based on Photonic Bandgap Amplifier," Photonics, 10, 965 (2023, August).
[15] Wang, Y., Set, S. Y. and Yamashita, S., "Active mode-locking via pump modulation in a Tm-doped fiber laser," APL Photonics 1(7) (2016).
[16] Cheng, H., Wang, W., Zhou, Y., Qiao, T., Lin, W., Guo, Y., Xu, S. and Yang, Z., "High-repetition-rate ultrafast fiber lasers," Optics Express 26(13), 16411 (2018).
[17] Kutz, J. N., Collings, B. C., Bergman, K., & Knox, W. H., "Stabilized pulse spacing in soliton lasers due to gain depletion and recovery," IEEE journal of quantum electronics, 34(9), 1749-1757 (1998).
[18] Korobko, D. A., Stoliarov, D. A., Itrin, P. A., Ribenek, V. A., Odnoblyudov, M. A., Petrov, A. B., & Gumenyuk, R. V. "Stabilization of a harmonic mode-locking by shifting the carrier frequency," Journal of Lightwave Technology, 39(9), 2980-2987 (2021).
[19] Stoliarov, D. A., Itrin, P. A., Korobko, D. A., Ribenek, V. A., Tabulina, L. V., Sysa, A. V., & Shaman, Y. P. "Saturable absorber based on the fiber coupler coated by CNTs," Optical Fiber Technology, 63, 102524 (2021).
[20] Bogusławski, J., Soboń, G., Zybała, R. and Sotor, J., "Towards an optimum saturable absorber for the multi-gigahertz harmonic mode locking of fiber lasers," Photonics Research 7(9), 1094 (2019).
[21] Chernysheva, M., Rozhin, A., Fedotov, Y., Mou, C., Arif, R., Kobtsev, S. M., & Turitsyn, S. K. (2017). Carbon nanotubes for ultrafast fibre lasers. Nanophotonics, 6(1), 1-30
[22] Lecaplain, C. and Grelu, P., "Multi-gigahertz repetition-rate-selectable passive harmonic mode locking of a fiber laser," Optics Express 21(9), 10897 (2013).
[23] Rana, F., Lee, H. L. T., Ram, R. J., Grein, M. E., Jiang, L. A., Ippen, E. P. and Haus, H. A., "Characterization of the noise and correlations in harmonically mode-locked lasers," Journal of the Optical Society of America B-optical Physics 19(11), 2609 (2002).
[24] Ribenek, V. A., Stoliarov, D. A., Korobko, D. A., & Fotiadi, A. A., "Mitigation of the supermode noise in a harmonically mode-locked ring fiber laser using optical injection," Optics Letters, 46(22), 5747-5750 (2021).
[25] Korobko, D. A., Ribenek, V. A., Stoliarov, D. A., Mégret, P., & Fotiadi, A. A., "Resonantly induced mitigation of supermode noise in a harmonically mode-locked fiber laser: revealing the underlying mechanisms," Optics Express, 30(10), 17243-17258 (2022).
[26] Nakazawa, M., Tamura, K. and Yoshida, E., "Supermode noise suppression in a harmonically modelocked fibre laser by selfphase modulation and spectral filtering," Electronics Letters 32(5), 461 (1996).
[27] Schröder, J., Alasia, D., Sylvestre, T., & Coen, S., "Dynamics of an ultrahigh-repetition-rate passively mode-locked Raman fiber laser," JOSA B, 25(7), 1178-1186 (2008).
[28] Korobko, D. A., Ribenek, V. A., Itrin, P. A., Stoliarov, D. A., & Fotiadi, A. A., "Polarization maintaining harmonically mode-locked fiber laser with suppressed supermode noise due to continuous wave injection," Optics & Laser Technology, 162, 109284 (2023).
[29] Ribenek, V. A., Stoliarov, D. A., Korobko, D. A., & Fotiadi, A. A. "Pulse repetition rate tuning of a harmonically mode-locked ring fiber laser using resonant optical injection," Optics Letters, 46(22), 5687-5690 (2021).
[30] Korobko, D. A., Ribenek, V. A., Itrin, P. A., Fotiadi, A. A., "Birth and annihilation of solitons in harmonically mode-locked fiber laser cavity through continuous wave injection," Optical Fiber Technology, 75, 103216 (2023).
[31] Semaan, G., Komarov, A., Salhi, M. and Sanchez, F., "Study of a harmonic mode lock stability under external continuous-wave injection," Optics Communications 387, 65–69 (2017).
[32] Chen, C. J., Wai, P. K. A., & Menyuk, C. R. (1992). Soliton fiber ring laser. Optics letters, 17(6), 417-419.
[33] Agrawal, G. P. (2000). Nonlinear fiber optics. Springer, Berlin, Heidelberg.
[34] Yulin, A. V., Skryabin, D. V., & Russell, P. S. J., "Four-wave mixing of linear waves and solitons in fibers with higher-order dispersion," Optics letters, 29(20), 2411-2413 (2004).
[35] Sylvestre, T., Coen, S., Emplit, P., & Haelterman, M., "Self-induced modulational instability laser revisited: normal dispersion and dark-pulse train generation," Optics letters, 27(7), 482-484 (2002).

[36] Quiroga-Teixeiro, M., Clausen, C. B., Sørensen, M. P., Christiansen, P. L., & Andrekson, P. A., "Passive mode locking by dissipative four-wave mixing," JOSA B, 15(4), 1315-1321(1998).
[37] Aleshkina, S. S., Fedotov, A. B., Коробко, Д. А., Stoliarov, D., Lipatov, D. S., Velmiskin, V. V., Temyanko, V. L., Kotov, L. V., Gumenyuk, R. and Likhachev, M. E., "All-fiber polarization-maintaining mode-locked laser operated at 980 nm," Optics Letters 45(8), 2275 (2020).
[38] Komarov, K. Komarov, A. Niang, F. Sanchez, "Nature of soliton interaction in fiber lasers with continuous external optical injection," Physical Review A 89(1), 013833 (2014).
[39] Gumenyuk, R., Okhotnikova, E. O., Philippov, V. N., Korobko, D. A., Zolotovskii, I. O. and Guina, M., "Fiber Lasers of Prof. Okhotnikov: Review of the main achievements and breakthrough technologies," IEEE Journal of Selected Topics in Quantum Electronics 24(3), 1–14 (2018).
[40] Sanchez, F., Grelu, P., Leblond, H., Komarov, A., Komarov, K., Salhi, M.,& Chouli, S., "Manipulating dissipative soliton ensembles in passively mode-locked fiber lasers," Optical Fiber Technology, 20(6), 562-574 (2014).
[41] Korobko, D. A., Gumenyuk, R., Zolotovskii, I. O., & Okhotnikov, O. G. "Multisoliton complexes in fiber lasers," Optical Fiber Technology, 20(6), 593-609 (2014).
[42] Korobko, D. A., Okhotnikov, O. G., & Zolotovskii, I. O., "Long-range soliton interactions through gain-absorption depletion and recovery," Optics letters, 40(12), 2862-2865 (2015).
[43] Fotiadi, A. A., Korobko, D. A., Zolotovskii, I. O., & Taylor, J. R. "Brillouin-like amplification in rare-earth-doped optical fibers," Optics Express, 29(24), 40345-40359 (2021).
[44] Panyaev, I. S., Itrin, P. A., Korobko, D. A., & Fotiadi, A. A., "Sub-100-Hz DFB Laser Injection-Locked to PM Fiber Ring Cavity," Journal of Lightwave Technology (2024).
[45] Fermann, M. E., & Hartl, I. Ultrafast fibre lasers. Nature photonics, 7(11), 868-874 (2013).
[46] Nishizawa, N. (2014). Ultrashort pulse fiber lasers and their applications. Japanese Journal of Applied Physics, 53(9), 090101.
[47] Zervas, M. N., & Codemard, C. A., "High power fiber lasers: a review," IEEE Journal of selected topics in Quantum Electronics, 20(5), 219-241 (2014).
[48] Li, X., Huang, X., Hu, X., Guo, X., & Han, Y., "Recent progress on mid-infrared pulsed fiber lasers and the applications," Optics & Laser Technology, 158, 108898 (2023).